

Quantitative analysis of the morphing wing mechanism of raptors: IMMU-based motion capture system and its application on gestures of a *Falco peregrinus*

Di Tang(唐迪), Liwen Zhu(朱力文), Wenxi Shi(施文熙), Dawei Liu(刘大伟), Yin Yang(杨茵), Guorong Yao(姚国荣), Senxiang Yan(严森祥), Zhongyong Fan(范忠勇), Yiwei Lu(陆祎玮), and Siyu Wang(王思宇)
Citation: Chin. Phys. B, 2024, 33 (**1**): 018701. DOI: 10.1088/1674-1056/ad0148
Journal homepage: http://cpb.iphy.ac.cn; http://iopscience.iop.org/cpb

What follows is a list of articles you may be interested in

Quantitative analysis of the morphing wing mechanism of raptors: Morphing kinematics of *Falco peregrinus* wing

Di Tang(唐迪), Jinqi Che(车婧琦), Weijie Jin(金伟杰), Yahui Cui(崔亚辉), Zhongyong Fan(范忠勇), Yin Yang(杨茵), and Dawei Liu(刘大伟)
Chin. Phys. B, 2023, 32 (**4**): 044703. DOI: 10.1088/1674-1056/aca201

Optical strong coupling in hybrid metal-graphene metamaterial for terahertz sensing

Ling Xu(徐玲), Yun Shen(沈云), Liangliang Gu(顾亮亮), Yin Li(李寅), Xiaohua Deng(邓晓华), Zhifu Wei(魏之傅), Jianwei Xu(徐建伟), and Juncheng Cao(曹俊诚)
Chin. Phys. B, 2021, 30 (**11**): 118702. DOI: 10.1088/1674-1056/abfb58

Detection of HIV-1 antigen based on magnetic tunnel junction sensors

Li Li(李丽), Kai-Yu Mak(麦启宇), Yan Zhou(周艳)
Chin. Phys. B, 2020, 29 (**8**): 088701. DOI: 10.1088/1674-1056/ab928d

Shape reconstructions and morphing kinematics of an eagle during perching manoeuvres

Di Tang(唐迪), Dawei Liu(刘大伟), Hai Zhu(朱海), Xipeng Huang(黄喜鹏), Zhongyong Fan(范忠勇), Mingxia Lei(雷鸣霞)
Chin. Phys. B, 2020, 29 (**2**): 024703. DOI: 10.1088/1674-1056/ab610a

---

Quantitative analysis of the morphing wing mechanism of raptors: IMMU-based motion capture system and its application on gestures of a *Falco peregrinus*

Di Tang(唐迪)[1,†], Liwen Zhu(朱力文)[1], Wenxi Shi(施文熙)[1], Dawei Liu(刘大伟)[2,‡], Yin Yang(杨茵)[2], Guorong Yao(姚国荣)[3], Senxiang Yan(严森祥)[3], Zhongyong Fan(范忠勇)[4], Yiwei Lu(陆祎玮)[4], and Siyu Wang(王思宇)[4]

[1] *College of Mechanical Engineering, Zhejiang University of Technology, Hangzhou* 310014, *China*
[2] *High Speed Aerodynamic Institute, China Aerodynamics Research and Development Center, Mianyang* 621000, *China*
[3] *Department of Radiation Oncology, The First Affiliated Hospital, Zhejiang University, Hangzhou* 310009, *China*
[4] *Zhejiang Museum of Natural History, Hangzhou* 310014, *China*

(Received 11 August 2023; revised manuscript received 22 September 2023; accepted manuscript online 9 October 2023)

This paper presented a novel tinny motion capture system for measuring bird posture based on inertial and magnetic measurement units that are made up of micromachined gyroscopes, accelerometers, and magnetometers. Multiple quaternion-based extended Kalman filters were implemented to estimate the absolute orientations to achieve high accuracy. Under the guidance of ornithology experts, the extending/contracting motions and flapping cycles were recorded using the developed motion capture system, and the orientation of each bone was also analyzed. The captured flapping gesture of the *Falco peregrinus* is crucial to the motion database of raptors as well as the bionic design.

Keywords: *Falco peregrinus*, IMMU-based, motion capture system, flapping gesture

PACS: 87.19.lu, 87.85.fk **DOI:** 10.1088/1674-1056/ad0148

1. Introduction

Analysis of wing kinematics is a key technique to study the biomechanical joint motion of nature birds. However, capturing the wing movement accurately is difficult because of the complex wing structure and the changeable flapping rules. At present, the existing motion capture system can not be effectively used in the motion capture of birds.

Motion capture system has been widely used in several application areas, such as medical rehabilitation, sports, film and television production and bionics research.[1] To identify the movement posture of the creature, the position, velocity, direction, and other information of the moving subject need to be accurately measured by certain attitude capture technology. At present, there are two commonly used motion capture technologies, optical-based and contact-based devices.[2] Optics-based devices capture video streams for analysis to determine sample motion. On the other hand, contact-based devices are precisely required to interact with the space of the sample. Based on the optical method, the sample usually does not need to install additional equipment due to the influence of external equipment on the sample motion. Samples can be more flexible with activities, but it is more susceptible to environmental disturbances such as occlusion, reflectance, and other environmental factors.[2] Furthermore, the equipment and operation process requirements are more stringent. In comparison, contact-based devices are easy to implement. Examples of contact-based devices are mobile touch screens, electromyographic (EMG)-based devices, and data gloves. The EMG-based device is portable, but the EMG signal is easily influenced by acquisition placement, individual differences, physical condition, and other factors.[3] Moreover, the movement of fine biological samples, especially birds, remains elusive. Attitude acquisition equipment such as an optical fibre sensor, pressure resistance sensor, pressure sensor, magnetometer, accelerometer, and gyroscope, to perceive movement.[4] This kind of method can well reflect the spatial motion trajectory, attitude and time series information of samples by capturing the information restricted by environmental conditions, such as the position, direction, and angle of samples. However, most products adopt wired data transmission mode, and the complex line will have a certain degree of influence on the movement of the sample itself, and the precision of the product needs to be improved. Therefore, developing a high-precision and lightweight attitude acquisition device with a wireless data transmission function for birds has become the goal of our research. As long as the frequency of data acquisition is increased, the device can obtain enough data to offset the impact of a small amount of data loss in the wireless transmission process, and the impact of the device on the attitude of the sample itself can be ignored. With the deepening

[†]Corresponding author. E-mail: tangdi@zjut.edu.cn
[‡]Corresponding author. E-mail: 13404019740@163.com

© 2024 Chinese Physical Society and IOP Publishing Ltd

of bionics research, the research requirements for the movement of biological samples are also further improved. Especially in the field of bionic aircraft, imitating and learning from the excellent flight posture of birds to obtain better flight performance is the basic idea of the design of morphological bionic aircraft. Bird flight posture has many characteristics, such as flexibility, changeability, and high frequency. Employing digital particle-image velocimetry, passerines have been found to control flight posture by coordinating tail and wing movements.[5] Three-dimensional (3D) laser scanners were used to reconstruct the shape of bird wings to analyze kinematics during flight.[6] Because birds use their wings in different ways in different flight movements, their roles in adjusting the position during complicated maneuvering remain largely unknown. At present, there are three main ways to study the flight posture of birds (as shown in Fig. 1), which are wind tunnel experiment observation, bird kinematics model calculation, and optical scanning. It is difficult to fully analyze the attitude of birds with the data obtained from the existing equipment. There are a few optically based devices that can capture bird pose under harsh conditions but can seriously lose data in complex environments, such as motion capture of birds moving through dense forests. Consequently, attitude acquisition equipment is developed to obtain accurate and usable bird attitude data. The above sensors measure the relative orientation of articulated segments by mounting the sensor across the joint of interest. Sensors are installed at specific locations to measure relative positions. Moreover, recalibration is necessary to mitigate estimation errors due to sensor displacements.

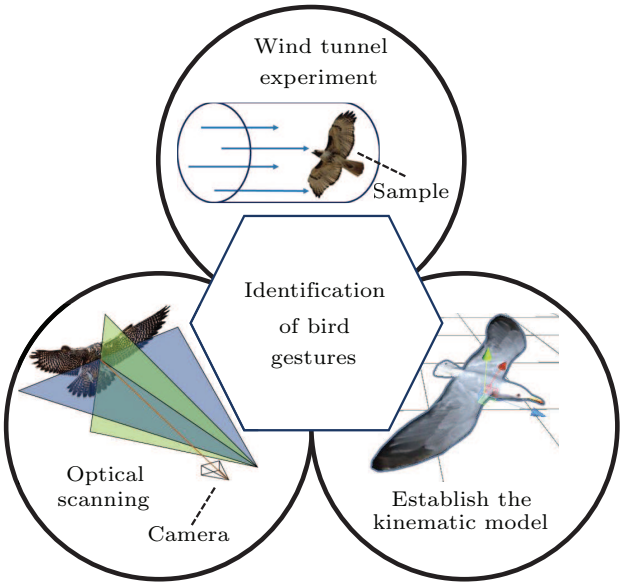


Fig. 1. Methods of bird posture study.

In the recent years, micro-electro-mechanical system (MEMS) technology has made a breakthrough in development. Compared with traditional sensors, micro inertial sensors have many advantages such as high precision, low cost, and small size. Conservatively, it can be used as a sensor to measure the attitude of birds and other special situations. Meanwhile, the magnetic sensor and inertial sensor are induced for accurate azimuth estimation. The inertial magnetic measurement unit (IMMU) has proven to be an accurate method for estimating sample orientation without additional optical equipment.[7] These devices are highly accurate, simple to control and intuitive to use. Furthermore, wearable inertial sensors and magnetic sensors are becoming increasingly popular in attitude acquisition.

The application of attitude sensors in bionics is still in its infancy. Motion capture devices based on micro inertial sensors can provide more accurate attitude results than other types of devices. Motion capture systems for the human body can generally be divided into three types, which are hand-held, wrist-wearable, and glove types. The KHU-l data glove[8] consists of six three-axis accelerometers, but it can only capture several kinds of gestures. The motion-capture system developed by Bor-Shing Lin is developed based on sixteen microinertia sensors.[1] It can capture the movements of each finger and palm, but the information on the heading angle is missing. The inertial and magnetic measurement unit is used by Filippo Cavallo, but it only uses four inertial and magnetic measurement units, which is unable to obtain information about each finger joint.[9] The development of the Power glove[10] includes six nine-axis micro-inertial sensors and ten six-axis micro-inertial sensors. The above motion capture systems are difficult to be applied to bird pose capture. For birds, these capture systems are too large to ensure accurate data, and the complex electrical wiring can have a great impact on the attitude of the bird itself. Therefore, a motion capture system using low low-power 9-axis motion tracking device has been developed, which can fully capture the movement information of birds during flight.

On the other hand, the IMMU-based device should be focused on the following two main aspects: calibration and fusion algorithm. Calibration is an important means to improve the performance of IMMU. Due to the differences in external signals, materials and other environmental factors, attitude sensors will inevitably produce errors, so calibration methods should be designed to improve accuracy. Therefore, the measurements of magnetometers are the combination of the earth's magnetic field and the extra magnetic field caused by the environmental effects. Hence, magnetometer calibration should be implemented to lessen the disturbance and improve the azimuth angle. The Kalman filter is a useful tool for sensor fusion. The extended Kalman filter is an efficient azimuth estimation method, which has been applied to many kinds of devices. Kalman filters have been shown to improve the estimation accuracy of data in wireless sensor networks with less computation.[11] Complementary filters are the high-pass sig-

nals provided by gyroscopes and the data from low-pass accelerometers and magnetometers which provide relatively accurate measurements at low frequencies fused to estimate the true orientation.[2]

Although systematic investigations of ornithopters for bionic bird flight have been undertaken for decades,[12] no aircraft can perfectly replicate the movements of birds. Part of the problem is that it is difficult to obtain precise and quantitative information about bird wing posture.[13] A broad consensus confirms that bird wing shapes are coordinated under the cooperation of muscles, skeletons, and nerves.[14] The motion capture device proposed is developed to capture bird motion data based on the IMMU-based motion capture system. The paper is organized as follows. Section 2 presents the designs of tiny motion capture devices with high accuracy. Section 3 describes the sensor calibration and attitude estimation algorithms, as well as the bird motion capture method. Section 4 reports calibration results, and bird motion capture experiments, which verify the accuracy of the proposed device. Section 5 gives the conclusions of the paper.

2. Hardware of IMMU-based motion capture system

2.1. Design of IMMU-based sensor

The development trend of the wireless measuring unit is higher precision with a small size in the current research. A control module and a transceiver module are always contained in a unit. However, the large geometry size will make it difficult to put the unit on the bird wing surface. Moreover, it is difficult to add more IMMUs with small distances to benefit from redundant measurements or gain more accurate measurements of wing motions. Here, The ICM-20948, with its 9-axis integration, on-chip digital motion processor (DMP), and runtime calibration firmware, is the world's lowest-power 9-axis motion tracking device. The devices are all integrated in a small 3 mm×3 mm×1 mm quad flat no-lead (QFN) package. Hence, it is suitable for the light-weight IMMU with high precision and low power consumption. Both the size and weight of the measuring unit can be dramatically reduced by introducing ICM-20948. Also, all electronic components are carefully arranged on the 4-layer PCB board. As a result, the developed tinny devices can be securely attached to the bird's wing, which makes it more accurate and easier to use. The reduction in equipment size also means that the equipment is less susceptible to external interference. The ICM-20948 sensor is welded on a solid PCB with dimensions of 20 mm×22 mm and a weight of 2.5 g, as shown in Fig. 2.

Connectivity is another important issue in the design. The wired networking approaches for the connections are convenient. However, it requires many electrical lines to be connected, and the complex electrical lines of the system will inevitably affect the wing posture and data authenticity. Thus, a wireless network approach is adopted in the system. Each sensor node contains a measuring module, a control module and a transceiver module. All measured data are transmitted from child sensor nods to the hub node in sequence through the transceiver module to ensure that each group of data is in the same moment of motion. Meanwhile, The microcontroller unit (MCU) only needs to read and send data from a single IMMU, reducing the complexity of the system and increasing the data transmission rate. Here the STM32F411 microcontroller and NRF52 microcontroller are used. Since all the sensor nodes operate independently and have no spatial connection, the sample can restore the gesture to the maximum extent.

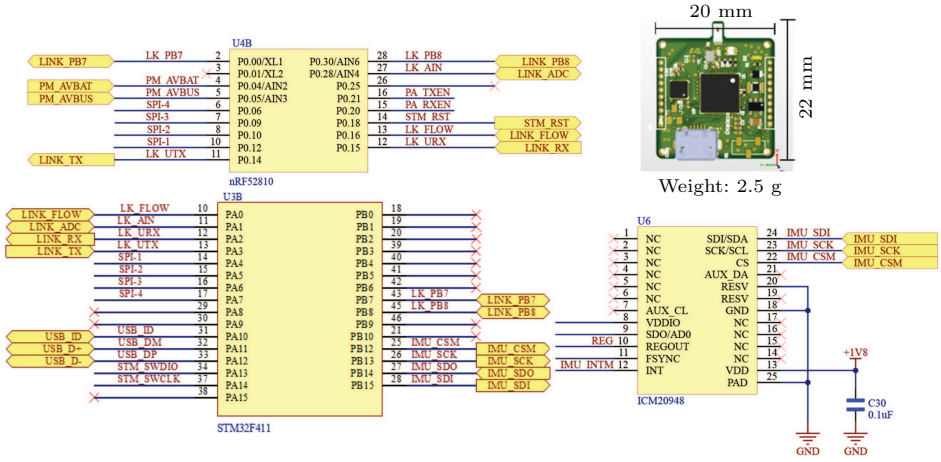


Fig. 2. The connection between the chips and the overall size.

2.2. Hardware of the motion capture system

After determining the IMMU-based measuring unit, the design of the motion capture system can be determined. There are several sending nodes and one receiving hub node in the motion capture system. Each node has an IMMU, which can be installed on the torso, head, humerus, radius, carpometacar-

pus, and tail feathers, depending on research requirements. The trunk node is used as the reference coordinate system, and the other nodes are used to measure the motions of the corresponding wing bone. The Li-pro battery is connected to the PCB board and separated by an insulating cooling layer. The block diagram of the motion capture system is shown in Fig. 3. The IMMUs' data was sampled, collected and computed by the MCU, and subsequently transmitted via bluetooth to the hub node. The MCU processes the raw data, and the quaternion obtained from each measurement node is encapsulated and sent to the PC. The baud rate for transmitting data was 115200 bps. Through this design, the motion capture system can display the bird's wing attitude change angle in real-time.

At present, there is no public report on the application of a motion capture system based on the nine-axis sensor to collect flight attitude information of birds in relevant research fields. The motion capture system with high accuracy but small size is designed to measure the natural wing motions. It is more compact, more durable, and more robust.

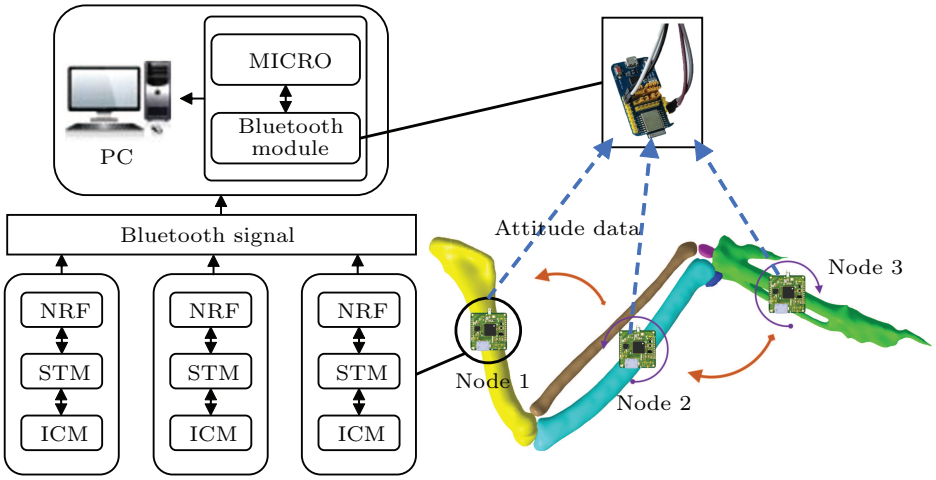


Fig. 3. System block diagram and 3D skeleton. Sensor nodes are installed on the 3D-printed bionic bone.

3. Measuring methods of the motion capture system

In this section, the capture methods are presented for the motion capture system. Sensor measurement method, calibration method and absolute orientations filter based on quaternion-based extended Kalman filter are described to implement the measurements of each unit. Thereafter, all the nodes are integrated to establish the motion capture system.

3.1. Models of the sensors

To fuse the inertial sensor and magnetic sensor, it is necessary to establish two coordinate systems. The orientations of a rigid body in the space are determined when the axis orientation of a coordinate frame attached to the body frame with respect to the navigation frame is specified.[2] The sensor models to be built include rate gyros, accelerometers, and magnetometers.

Because the MEMS rate gyros do not have enough sensitivity to measure the earth's angular velocity, the rate gyros model can get rid of the earth's angular vector. The output signal of a rate gyro is influenced by noise and bias:

$$\omega_{\mathrm{m}} = \omega + b_{\mathrm{g}} + w_{\mathrm{g}}, \tag{1}$$

where ω_{m} is measured by the rate gyros, ω is the true value, b_{g} is the gyro' bias, and w_{g} is the noise that is supposed to be Gaussian with zero means.

As the accelerometers model, the measurements of accelerometers in the body frame b can be written as follows:

$$a_{\mathrm{m}} = C_{\mathrm{n}}^{\mathrm{b}} M^{\mathrm{a}} (a + g) + b_{\mathrm{a}} + w_{\mathrm{a}}, \tag{2}$$

where a_{m} is 3×3 matrixes measured by the accelerometers, $C_{\mathrm{n}}^{\mathrm{b}}$ denotes the orientation cosine matrix representing the rotation from the navigation frame to the body frame, g and $a \in R^3$ are the gravity vector and the inertial acceleration of the body, respectively, expressed in the navigation frame, and $g = 9.81$ m/s^2 denotes the gravitational constant; M^{a} is 3×3 matrixes that scale the accelerometers outputs; b_{a} is the vector of accelerometers' bias; $w_{\mathrm{a}} \in R^3$ is the vector of Gaussian with zero-means. Commonly, the absolute acceleration of the rigid body in the navigation frame is supposed to be weak $a \ll g$ or the rigid body is static. Then, the model of accelerometers can be simplified as follows:

$$a_{\mathrm{m}} = C_{\mathrm{n}}^{\mathrm{b}} M^{\mathrm{a}} g + b_{\mathrm{a}} + w_{\mathrm{a}}. \tag{3}$$

As the magnetometers model, the unit vector H_{h} represents the ideal magnetic vector in the navigation frame. The measurements in the body frame b are defined

$$h_{\mathrm{m}} = C_{\mathrm{n}}^{\mathrm{b}} M^{\mathrm{h}} H_{\mathrm{h}} + b_{\mathrm{h}} + w_{\mathrm{h}}. \tag{4}$$

3.2. Extended Kalman filter

White noise, disturbance, *etc.*, are usually included in the measured data which will affect the accuracy of data. Therefore, calibration and filter design are needed. An extended Kalman filter is designed to estimate the orientation of bird wing bones. This approach has gained a high degree of recognition for vehicle and satellite[15] azimuth estimation, and more recently, MEMS-based IMMS tracking.[16–19] It is advantageous to ordinary extended Kalman filtering because differences in estimated and true orientation are assumed to be much smaller than the actual one, which eventually results in a smaller linearization error.[10] The multiplicative error quaternion method is used, and the error quaternion is represented as an unconstrained vector where the filter acts on the quaternion. Parameterization of the true quaternion q_{ij} is given by

$$q^{ij} = \bar{q}^{ij} \odot \delta q, \tag{5}$$

where $\bar{q}^{ij}$ is the nominal quaternion and δq is the error quaternion, $\odot$ is the quaternion multiplication operator. The helix angle $\delta\theta^{ij}$ can approximate the error quaternion:

$$\delta q \approx \left[a\frac{1}{2}\delta\theta^{ij}\right]^{\mathrm{T}}, \tag{6}$$

where θ^{ij} is the unit vector indicating a rotation axis and δ is the magnitude of the rotation around the axis. Filters are deployed at each sensor node. The sensor is updated according to the measured accelerometer, magnetometer and biomechanical dimensional information. The filter uses a general state space model for dynamics x_{k+1} and measurements y_k:

$$x_{k+1} = f(x_k) + v, \tag{7}$$

$$y_k = h(x_k) + e, \tag{8}$$

where $f(x_k)$ denotes the transition function and $h(x_k)$ denotes the measurement function. After the sensor status is initialized, the filter receives data from each sensor node and performs an iterative calculation of updates. Measurement updates y_{vector} are differentiated from accelerometers and magnetometers, while biomechanical information is represented by y_{biomech}. In each iteration calculation, the Kalman gain is calculated, the error state and its covariance are updated according to Ref. [20].

$$K_k = P_k^- H_k^{\mathrm{T}} \left[H_k P_k^- H_k^{\mathrm{T}} + R_K\right]^{-1}, \tag{9}$$

$$P_k^+ = [I - K_k H_k] P_k^-, \tag{10}$$

$$\delta\hat{x}_k^+ = \delta\hat{x}_k^- + K\left[\delta y - h\left(\delta x_k^-\right)\right], \tag{11}$$

where the minus and plus sign denote the a-priori and a-posteriori estimate respectively, H denotes the linearized matrix of the measurement equation $h(\delta x)$, I is an identity matrix, R is the measurement covariance corresponding to the measurement uncertainty, δy is the difference between estimated and measured sensory input.

3.3. Motion capturing system

For bird body structure, the articular wing skeleton can be modelled as a closed chain, originating from the trunk and ending at the carpometacarpus, as illustrated in Fig. 4. Hummers, radius, ulnar, and carpometacarpus are included in the wing skeleton. The four main bones are modelled as rigid bones with four sensors mounted on the covered feathers. The trunk sensor lies on the torso dorsal with the X axis directing ahead, and the Y axis directing from the torso to the wingtip. All the other sensors are placed and aligned with the trunk sensor at the initial state. The relative orientation between the two neighbouring bones can be obtained by solving the following differential equation:

$$\dot{q}^{ij} = q^{ij} \odot \frac{1}{2}\omega_{ij}^{j}, \tag{12}$$

where q_{ij} is the unit quaternion describing the orientation of frame Ψ_j with respect to frame Ψ_i,[21] and ω_{ij}^{j} is the angular velocity of body j with respect to Ψ_i expressed in frame Ψ_j. The relative angular velocity ω_{ij}^{j} is determined by subtracting the absolute angular velocity of the two bones. The angular velocity of a single body is measured using a 3D rate gyroscope,[10] whose output y_Ω can be modelled as

$$y_\Omega^{\mathrm{b}} = \omega_{\mathrm{Gb}}^{\mathrm{b}} + b_\Omega^{\mathrm{b}} + e_\Omega, \tag{13}$$

where $\omega_{\mathrm{Gb}}^{\mathrm{b}}$ is the angular velocity of the body with respect to a global frame expressed in the body frame, b_Ω^{b} is a slowly varying sensor bias and e_Ω is independent identically distributed white Gaussian noise. The relative angular velocity of two adjacent bones can be expressed as

$$\omega_{ij}^{j} = \left(y_\Omega^j - b_\Omega^j - e_\Omega^j\right) - R^{ji}\left(y_\Omega^i - b_\Omega^i - e_\Omega^i\right). \tag{14}$$

Before measuring the bird's posture, sensor 1 was fixed on the torso, and sensors, 2, 3, and 4 were fixed on the left humerus, ulnar, and carpometacarpus, and were as close to the centre of the bone as possible. The increase in the number of sensors is helpful to the improvement of data accuracy to some extent. In this experiment, the size of the sample limits the number of sensors. If it is used for large birds, the number of sensors can be appropriately increased. Similarly, sensor units 5, 6, and 7 were fixed on the right wing. It should be noted that the small size of the radius makes it difficult to be identified by the developed sensor, thus, only ulna motion is measured in the current research. The bird wing is simplified as a set of linked mechanisms, where the humerus is modeled as part 1, the union of radius and ulna are modeled as part 2, and the carpometacarpus is modeled as part 3, as shown in Fig. 4.

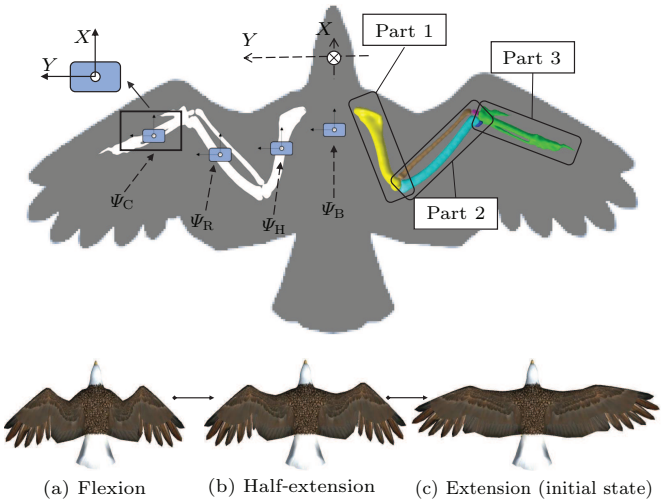


Fig. 4. Illustration of sensor arrangement. Sensors are installed on the skin above the humerus (H, part 1), radius (R, part 2), carpometacarpus (C, part 3) and body (B).

3.4. Sensor accuracy verification

To verify the measurement data of the motion capture system, the static angle accuracy and dynamic angle accuracy of the motion capture system were tested. The sensor node was tested on an Instrumentation System TVP-352A with a measuring range of 0°–360° and angular accuracy of $\pm 1''$. An electronic timer with a deviation of ± 0.1 s/h was also used for angular accuracy. During the test, the ambient temperature in the laboratory was 21 °C and the air humidity was 55%. The sensor was mounted tightly on the testing platform and moved in sync with the platform, as shown in Fig. 5. Both the measured data of the sensor and standard data of the TVP-352A were transmitted from the MCU to the computer at the same time.

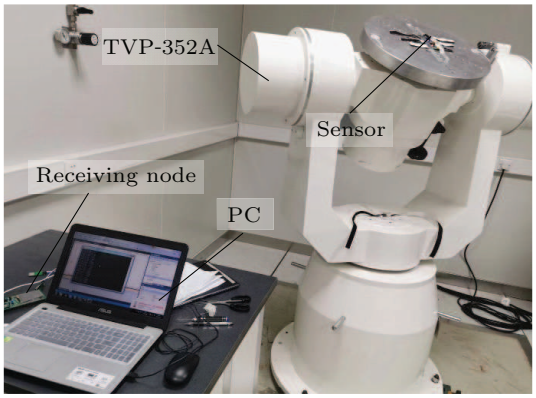


Fig. 5. Arrangement of the precision measurement for the developed sensor.

Table 1. Static angle measurement results.

Number	Measuring point (°)	Reference value (°)	Measured value (°)	Error (°)
1	$0 \sim -10$	-10.00	-10.03	-0.03
2	$-10 \sim -20$	-10.00	-9.91	0.09
3	$-20 \sim -30$	-10.00	-9.98	0.02
4	$-30 \sim -40$	-10.00	-9.95	0.05
5	$-40 \sim -50$	-10.00	-10.04	-0.04
6	$-50 \sim -60$	-10.00	-9.94	0.06
7	$-60 \sim -70$	-10.00	-10.08	-0.08
8	$-70 \sim -80$	-10.00	-10.00	0.00
9	$-80 \sim -90$	-10.00	-10.10	-0.10

Table 2. Dynamic angle measurement results.

Number	Minimum angular velocity (°/s)	Maximum angular velocity (°/s)	Reference value (°/s)	Maximum error (°/s)
1	9.61	10.29	10.00	-0.39
2	9.54	10.25	10.00	-0.46
3	9.59	10.30	10.00	-0.41
4	9.56	10.32	10.00	-0.44

As the angular accuracy test, the sensor was rotated from 0° to 90°, and angular was recorded at 9 critical stations. Deviations of the measured data from the standard data are illustrated in Table 1. It is shown that the maximum deviation is $-0.1°$. As the angular velocity accuracy test, four test cases were performed under 10.00 °/s. A maximum deviation of -0.46 °/s was found as shown in Table 2. The maximum deviations of both angular and angular velocity are small and the tested data match with the standard data well. Above all, the accuracy of the developed sensor has been verified.

4. Morphing experiment of a *Falco peregrinus*

4.1. Experimental arrangement

Motion capture experiments of *Falco peregrinus* were conducted because it is one of the world's fastest birds. They are strong, fast, and ferocious, they hunt by clenched talons and kill by impact using their high speed and maneuverability.[22] Many investigations have contributed to

the avian anatomy of the muscles and bones.[23–26] A carcass of *Falco peregrinus* was donated by the Zhejiang Museum of Natural History as detailed in our previous research.[22]

In our previous studies, bird specimens were carried out in a fixed posture using a CT scan approach. Detailed gestures, including bone shapes, and relative rotations, *etc*., were all obtained with high precision. However, the previous postures were measured in several discrete positions, and no continuous motions have been obtained. To estimate the wing motions in a continuous manner, the developed motion capture system was used to implement this measurement. The specimen was suspended in a developed suspension system which was detailed in our previous research.[22] Pairs of nylon wires were used to suspend each wing to maintain the exact flying pose. The specimen shapes were manually adjusted to morph under the professional directions of the ornithologists of the Zhongyong Fan team. The flapping and extending movements of *Falco peregrinus* were recorded by each sensor unit, and the corresponding critical postures were also scanned by the CT approach, as shown in Fig. 6. The bird wing was simplified as a set of linked mechanism and motions of ulna and carpometacarpus were obtained. After the experiment, the testing bed was cleaned and disinfected to guarantee biosafety. One limitation of this experiment is that the motion of the sample is different from its natural state, only the geometric pose data has reference value, and the dynamic information such as acceleration and frequency cannot be reproduced through the dead body sample. More valuable dynamic information needs to be collected in future studies involving live samples for a more complete understanding. In this regard, experiments have verified the applicability of the developed sensor, and it is planned to be applied to the live motion capture of small birds such as pigeons and parrots. To obtain reliable dynamic data such as acceleration and frequency.

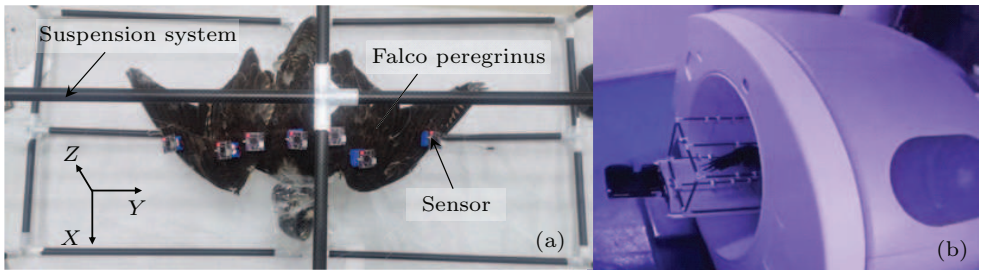


Fig. 6. Experimental arrangement of *Falco peregrinus*. (a) The specimen was suspended in the suspension system with the sensor mounted, (b) critical postures were scanned.

4.2. Extending motion

The continuous extending motions of the *Falco peregrinus* wing were recorded, as shown in Fig. 7(a). Sinusoidal function appeared in both ulna and carpometacarpus rotations. The roll angle (rotate around X axis) and pitch angle (rotate around Y axis) of the skeleton remained almost the same during the extension. Rotation around the Z axis is the main

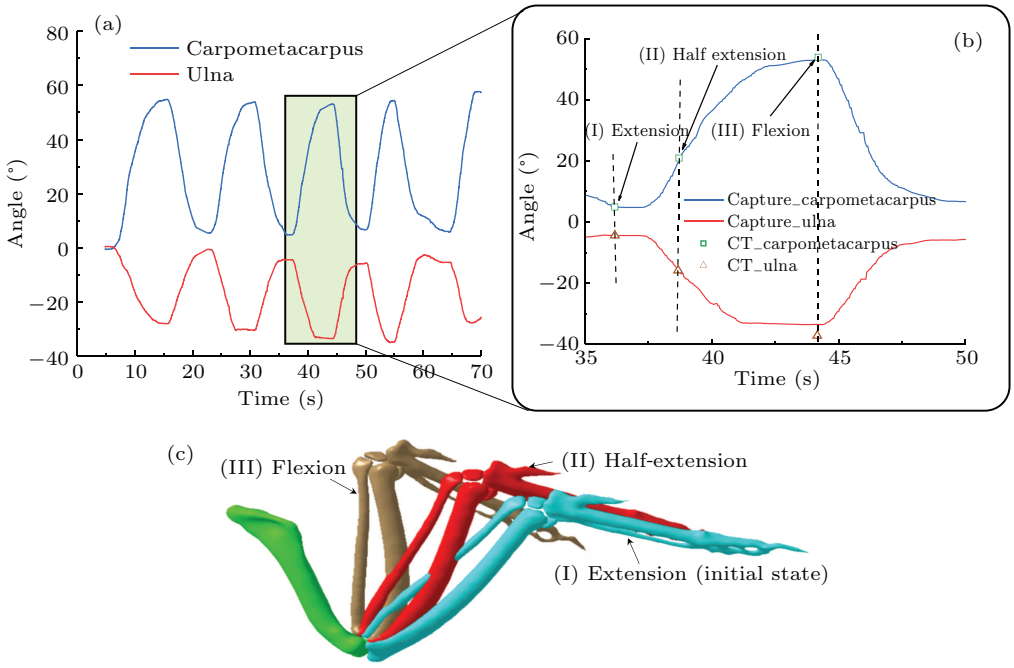


Fig. 7. Captured motion and scanned shape of the falcon wing: (a) continuous rotations of ulna and carpometacarpus, (b) scanned bone shape, (c) comparison of scanned angle and captured motion.

factor to change the wing shape. Only a minus rotation was found for the humerus which always fluctuated by the cover feathers. Thus, it was not discussed in the current research. The measurement results show that the motion of the carpometacarpus is the key factor in wing shape during the extending/contracting motion. It is shown that the extreme rotation of the ulna is -35.1° and the one of carpometacarpus is 57.7°. During extension, three critical postures, extension, half-extension and extraction, were also scanned by CT approach, as shown in Fig. 7(c). Thereafter, the orientation of each bone was extracted from the scanned shape and then compared in Fig. 7(b). It is shown that the two results are consistent with each other, and the validity of the measured data is verified.

4.3. Flapping motion

A typical flapping motion of *Falco peregrinus* was discussed in the current research. A three-jointed arm system is usually adopted for avian wing geometry and kinematic analysis. However, the cover feathers were stacked up and the orientation of the sensor above the humerus severely fluctuated when the wing was fully contracted. Thus, a discussion about humerus motion was not presented, and a simple double-jointed arm system was used to estimate wing flapping motions as shown in Fig. 8(a). In detail, the humerus, radius and ulna were integrated as arm 1, while the carpometacarpus was simplified as arm 2. The study focused on rotations of arm 1 and arm 2 which reflected the manoeuvre ring motions of the *Falco peregrinus*. On the other hand, no experimental motion data has ever been reported for nature *Falco peregrinus*. Tianshu Liu once extracted and estimated the flapping wing movement data of the seagull by optical means.[27] In consideration that the body length, weight, and wingspan of *Falco peregrinus* are similar to those of a seagull, the motions of the *Falco peregrinus* were compared according to the seagull's motions.[27]

During the test, the wing shape of *Falco peregrinus* was found to change dramatically during a flapping cycle, which was mainly contributed by the rotation of the shoulder joint, the angle between the ulna and carpometacarpus was also found to oscillate with an impressive amplitude. The recorded periodic movements of *Falco peregrinus* were consistent with those of the seagull as well as each bone. In downstroke, the wing extends as far as possible to attain a large surface which is beneficial to promote more air. During the downstroke, more lift and thrust were generated to resist gravity and drag. As the wing was raised during the upstroke, the carpometacarpus was slightly contracted towards the torso to reduce the surface area and minimize air resistance.[28]

Based on the experimental results, the established raptor model was used to restore the wing posture. Figure 9 illustrates the changes in flapping wing attitude over one cycle. By coupling the data to the model, we can directly observe the posture of the wings when they flutter. During the downstroke, the wings are extended as far as possible to expand the wing area, and secondary flight feathers are stacked in sequence to cover the trailing edge of the wings, which helps to increase the lift and thrust obtained. During the upstroke, the wing humerus and ulna (arm 1) lift first, while the carpometacarpal (arm 2) folds downward and contracts inward. When arm1 lifts near the highest point, arm 2 lags behind arm 1 and extends. At the same time, the gap between the secondary flight feathers is enlarged, which increases the air leakage rate during the upstroke. Therefore, the air resistance during the upstroke is greatly reduced. Thanks to a series of variants, the wings gain lift and sustained thrust for flight during the entire flapping cycle.

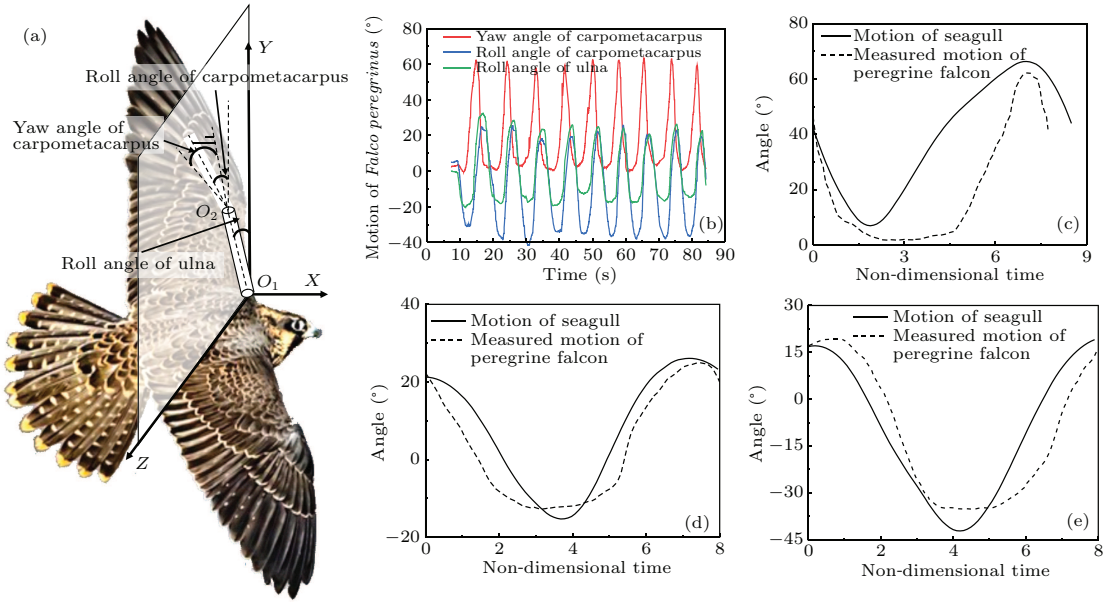


Fig. 8. Measured motion of the *Falco peregrinus*: (a) flapping motion of the main bones of Falco peregrinus, (b) motion of *Falco Peregrinus*, (c) yaw angle of carpometacarpal, (d) roll angle of ulna, (e) roll angle of carpometacarpal.

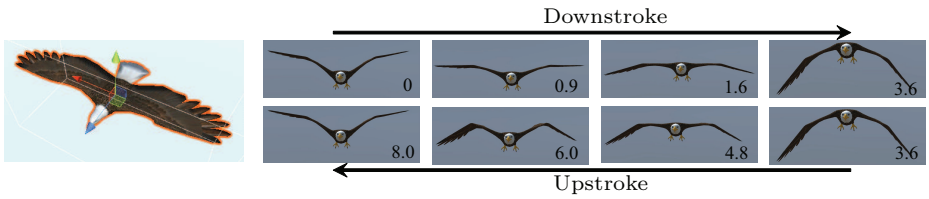


Fig. 9. Raptor model and flapping posture recovery.

5. Conclusion

No wing motion experiment has been reported for nature *Falco peregrinus* which is critical for studying bird flights and bionic design. Thus, a novel tinny motion capture system was developed for birds, and wing motions of a *Falco peregrinus* were recorded. In this study, we evaluated the performance of the sensors as well as the flight attitude of the peregrine falcon.

Both hardware and software of measurement sensor that is made up of micromachined gyroscopes, accelerometers, and magnetometers have been designed and implemented. The measured data of each sensor node is fused to obtain quaternions based on an extended Kalman filter and then transmitted to the hub node using a Bluetooth module. All the nodes are integrated to establish the motion capture system with high accuracy verified on an instrumentation system TVP-352A.

Thereafter, wing motions of a *Falco peregrinus* were measured using the developed motion capture system. The extending/contracting motions were recorded in a continuous manner to study the morphing process from cruising to diving. Three critical postures of the wings, extension, half-extension and extraction were verified using a CT scan approach. Then, the flapping cycles of the falcon were also studied based on a two-jointed arm model. Combined with the model and data, the flapping wing cycle was reconstructed, and the causes of high and low lift in the process of peregrine falcon flapping were verified. The results of the motion capture experiment meet the expected standards. Therefore, the lightweight IMMU-based motion capture system is considered suitable for the movement data collection of living birds such as pigeons and parrots. The next stage is to test motion capture on live pigeons with the capture system developed. This helps to advance the study of the flight mechanism of birds and can be mutually verified with optical motion capture methods.

The attitude capture system designed in this article is available in the future of the natural action of birds. In addition, the wing kinematics given in this paper can be used for the preliminary design of flapping MAVs, and they provide a foundation for further experimental and computational studies to understand the aerodynamic aspects of flapping flight.

Acknowledgements

Project supported by the National Natural Science Foundation of China (Grant Nos. 52175279 and 51705459), the Natural Science Foundation of Zhejiang Province, China (Grant No. LY20E050022), and the Key Research and Development Projects of Zhejiang Provincial Science and Technology Department (Grant No. 2021C03122).

References

[1] Lin B S, Lee I J, Hsiao P C, Yang S Y and Chou W 2014 *Tenth International Conference on Intelligent Information Hiding and Multimedia Signal Processing* 25
[2] Fang B, Sun F C, Liu H P and Guo D 2017 *Seientific Programming* **2017** 7594763
[3] Li Y, Chen X, Zhang X, Wang K Q and Wang Z J 2012 *IEEE Trans. Biomed. Eng.* **59** 2695
[4] Dipietro L, Sabatini A M and Dario P 2008 *IEEE Trans. Sys. Man Cyber. Capplications and Reviews* **38** 461
[5] Su J Y, Ting S C, Chang Y H and Yang J T 2012 *J. Royal Soc. Interface* **9** 1674
[6] Tang D, Liu D W, Zhu H, Huang X P, Fan Z Y and Lei M X 2020 *Chin. Phys. B* **29** 024703
[7] Roetenberg D, Luinge H J, Baten C T M and Veltink P H 2005 *IEEE Transactions Neural Systems and Rehabilitation Engineering* **13** 395
[8] Kim J H, Thang N D and Kim T S 2009 2009 *IEEE International Symposium on Industrial Electronics* 1013
[9] Cavallo F, Esposito D, Rovini E, Aquilano M, Carrozza M C, Dario P, Maremmani C and Bongioanni P 2013 2013 *IEEE 13th International Conference on Rehabilitation Robotics (ICORR)* 1
[10] Kortier H G, Sluiter V I, Roetenberg D and Veltink P H 2014 *Journal of Neuroengineering and Rehabilitation* **11** 70
[11] Huang J W and Feng J C 2014 *Chin. Phys. B* **23** 070504
[12] Huang M Y 2019 *Proceedings of the Institution of Mechanical Engineers Part G-Journal of Aerospace Engineering* **233** 3260
[13] Parslew B 2015 *Journal of the Royal Society Interface* **12** 20140953
[14] Crandell K E and Tobalske B W 2011 *Journal of Experimental Biology* **214** 1867
[15] Crassidis J L, Markley F L and Cheng Y 2007 *Journal of Guidance Control and Dynamics* **30** 12
[16] Yun X P and Bachmann E R 2006 *IEEE Transactions on Robotics* **22** 1216
[17] Sabatini A M 2006 *IEEE Transactions on Biomedical Engineering* **53** 1346
[18] Roetenberg D, Slycke P J and Veltink P H 2007 *IEEE Transactions on Biomedical Engineering* **54** 883
[19] Luinge H J, Veltink P H and Baten C T M 2007 *Journal of Biomechanics* **40** 78
[20] Gustafsson F 2010 *Statistical Sensor Fusion* (Sweden: Studentlitteratur AB) 9789144054896
[21] Kuipers J B 2002 *Quaternions and Rotation Sequences* (Princeton: Princeton University Press) 9780691102986
[22] Tang D, Huang X P, Che J Q, Jin W J, Cui Y H, Chen Y J, Yuan Y X, Fan Z Y, Lu W W, Wang S Y, Yang Y and Liu D W 2022 *Fundamental Research*
[23] Yu M K, Wu P, Widelitz R B and Chuong C M 2002 *Nature* **420** 308
[24] Hieronymus T L 2016 *J. Anat.* **229** 631
[25] Ponitz B, Triep M and Brücker C 2014 *Open J. Fluid Dyn.* **4** 363
[26] Baier D B, Gatesy S M and Dial K P 2013 *PLoS One* **8** e63982
[27] Liu T S, Kuykendoll K, Rhew R and Jones S 2006 *AIAA Journal* **44** 954
[28] Tang D, Fan Z Y, Lei M X, Lv B B, Yu L and Cui H 2019 *Chin. Phys. B* **28** 034702